(This is a sample cover image for this issue. The actual cover is not yet available at this time.)

Journal of Nuclear Materials 420 (2012) 116–122

Contents lists available at SciVerse ScienceDirect

Journal of Nuclear Materials

journal homepage: www.elsevier.com/locate/jnucmat

X-ray absorption studies of bismuth valence and local environments in borosilicate waste glasses

David A. McKeown *, Hao Gan, Ian L. Pegg

Vitreous State Laboratory, The Catholic University of America, 620 Michigan Ave., N.E., Washington, DC 20064, United States

ARTICLE INFO

Article history:
Received 6 July 2011
Accepted 21 September 2011
Available online 29 September 2011

ABSTRACT

X-ray absorption spectra (XAS) were collected and analyzed to characterize bismuth (Bi) environments in borosilicate glass formulations developed for the immobilization of high level nuclear wastes (HLW), from the bismuth phosphate process. Therefore, the structural role of Bi in these glasses is of interest; in addition in the present study, more particular interest in Bi originated from unusual foaming that was observed during melt cooling, where it was initially suspected that Bi^{3+} reduction to Bi^0 may generate oxygen that caused the foaming. Observations from scanning electron microscopy of some HLW glass samples indicated a Bi-phosphate association. Bi L_{III} XAS of 13 Bi-containing waste glass formulations of various compositions were measured that exhibited varying degrees of melt foaming. The Bi XAS are similar for all glasses investigated, and indicate $Bi^{3+}O_3$ nearest-neighbor environments with Bi–O distances near 2.13 Å. This environment is similar to the most localized Bi coordination characteristics in the crystalline Bi-silicates, eulytite ($Bi_4Si_3O_{12}$) and bismutoferrite ($BiFe_2Si_2O_8OH$). However, the Bi-environments in the glasses are distinctly different from the Bi-site in crystalline $BiPO_4$; therefore, XAS indicates no evidence of Bi-phosphate domains in the glasses measured. No XAS evidence was observed in any of the glasses investigated for Bi clustering, such as metallic Bi, or Bi–O–Bi bonding. Since the local Bi environments look similar for all glasses investigated, Bi XAS data and analyses show no association of the melt foaming problems with changes of Bi environments in the corresponding glass. The foaming may be dependent on chromate or phosphate behavior in the glass structure.

1. Introduction

The chemical and structural roles of bismuth (Bi) in borosilicate melts are of interest with regard to the vitrification of high-level radioactive wastes. High-level waste (HLW) streams from very early nuclear fuel reprocessing flow-sheets, such as some of the defense wastes in storage at the Hanford site in the United States, contain significant amounts of Bi. The structural role of Bi in these glasses is therefore of interest. In addition, in the present study, more particular interest in Bi originated from unusual foaming behavior that was observed during cooling of Bi-containing glass melts according to the thermal profile expected after filling of a full-scale HLW canister (the so-called center-line canister cooling (CCC) profile) [1]. In reviewing potential origins of this behavior, one considered hypothesis was that Bi^{3+} reduction to Bi^0 may cause oxygen generation and the foaming. In response to this issue, new glass formulations were synthesized, with variations in the concentrations of Bi_2O_3 and other components, namely, P_2O_5 and Cr_2O_3, that were also suspected of being linked to the observed foaming and possible changes in Bi behavior. Structural information obtained from X-ray absorption spectroscopy (XAS) on these Bi-containing HLW glasses has the potential to provide insights into any Bi-related atomic structural origins of the observed melt foaming that could lead to adjustments in glass chemistry or changes in operating procedures that may reduce or eliminate melt foaming.

An X-ray absorption spectrum is divided into two regions: the X-ray absorption near edge structure (XANES) that includes an absorption edge of the element of interest and the extended X-ray absorption fine structure (EXAFS). The slope of the absorption edge rise, and corresponding edge energy is sensitive to the valence of the absorbing element, where the edge energy increases with higher valence. Features at the absorption edge are also sensitive to the coordination environment surrounding the absorber (in this case Bi). The EXAFS data, by convention, are extracted from a spectrum at approximately 20 eV beyond the absorption edge to higher energies. In many cases, EXAFS oscillations are due primarily to single scattering of the spherical electron wave emitted by the absorber from the surrounding arrangement of atoms. The EXAFS data are analyzed to quantitatively determine average bond distance (r (Å)), coordination number (n (atoms)), and disorder (Debye–Waller factor or σ^2 (Å^2)) of shells of atoms around the absorber.

* Corresponding author. Tel.: +1 202 319 5226; fax: +1 202 319 4469.
E-mail address: davidm@vsl.cua.edu (D.A. McKeown).

0022-3115/$ - see front matter © 2011 Elsevier B.V. All rights reserved.
doi:10.1016/j.jnucmat.2011.09.018

Scanning electron microscopy (SEM) analyses of some CCC samples identified micron-scale Bi-containing phosphate phases. This raises the possibility of Bi segregation to phosphate-rich domains within the glass. In this case, Bi–O distances determined from EXAFS may indicate whether Bi is in phosphate- or silicate-rich domains within a glass. Bi–O nearest-neighbor distances in crystalline silicates range from 2.05 to 2.22 Å [2–4], while crystalline $BiPO_4$ has considerably longer Bi–O distances from 2.33 to 2.68 Å [5]. If the Bi environments in silicate glasses follow the trends in the above crystalline phases, EXAFS determined Bi–O distances for the glasses should indicate whether Bi is surrounded by SiO_4 or PO_4 tetrahedra.

The borosilicate samples studied are chemically complex and have Bi_2O_3 concentrations ranging from 11.2 to 6.9 wt.% (Table 1). The F-series glasses had varying degrees of melt foaming problems: the worst foaming sample was HLW-Bi-F2, while three other samples, HLW-Bi-F3, -5r, and -F8, had foaming minimized. From initial Raman and SEM observations, Bi behavior in these samples differs from that observed for binary Bi-silicate glasses [6–8]. In light of the Bi-to-phosphate correlation found in some of the CCC samples and the possible correlation of these elements to foaming, three additional glasses were made where the Bi_2O_3- and P_2O_5-contents were varied independently: a P_2O_5-free glass (HLW-Bi-P0), a glass with twice the P_2O_5-content (HLW-Bi-2P), and a glass with twice the Bi_2O_3-content (HLW-Bi-2Bi). The Raman spectra of these glasses show chromate Cr–O stretch modes decrease intensity with increasing P_2O_5 content, which indicates a possible phosphate–chromate interaction in the glass formulations [9]. As a result, a glass was synthesized and measured with twice the original P_2O_5 content and no Cr_2O_3 (HLW-Bi-2P0Cr).

Melt foaming for some of the formulations studied could also be correlated to the presence of chromium (Cr) and the crystallization of Cr-spinels (see Table 1). Raman active Cr–O stretch chromate modes from the glass were not present when spinel crystallization took place. These observations support the hypothesis that the absence of Cr^{6+} in chromate was due to the reduction of Cr^{6+} to Cr^{3+} and its incorporation into spinel crystals during cooling of the melt; this process provides a second mechanism that could generate oxygen and cause the observed foaming. Accordingly, foaming was minimized in melts for formulations F3 (HLW-Bi-F3), F5r, and F8, where chromate modes are observed in the Raman spectra with no evidence of spinel (either by Raman or XRD). Conversely, however, one of the formulations that showed the worst foaming, HLW-Bi-F2, exhibited chromate modes and no spinel crystals. The focus of the present work, however, is on investigating the local environment of Bi in these glasses and the potential role of Bi, if any, in the observed foaming behavior.

Bi acts as a silicate tetrahedral network modifier in crystalline silicates [2–4]; therefore, a similar role in borosilicate glass structure is anticipated. The Bi^{3+}-sites in these phases have asymmetric coordination environments due to lone pair electrons that extend in one direction from each Bi. XAS spectra were collected for the crystalline Bi-silicates, eulytite ($Bi_4Si_3O_{12}$) [2] and bismutoferrite ($BiFe_2Si_2O_8OH$) [3], as well as crystalline $BiPO_4$ (monazite structure [5]). In eulytite and $BiPO_4$, SiO_4 and PO_4 tetrahedra, respectively, are isolated from each other by Bi^{3+} [2,5]. Bi in the eulytite garnet-type structure is surrounded by six oxygens [2]: three at 2.15 Å and another three at 2.62 Å. Bismutoferrite is a layer structure [3], where Bi is bonded between octahedral $FeO_4(OH)_2$ and silicate layers. There are two sets of Bi–O distances to the Fe-octahedra: two at 2.05 Å and another at 2.22 Å. Six Bi–O bonds are found between Bi and oxygens in the silicate layer, that range from 3.28 to 3.43 Å. In $BiPO_4$, there are eight different Bi–O distances ranging from 2.33 to 2.68 Å [5].

Several structural investigations concerning the reduction of Bi in binary silicate glasses have been reported [6–8,10,11], where Bi_2O_3 concentrations were as high as 50 mol%. A Si MAS-NMR and X-ray scattering study of $x(Bi_2O_3)\cdot(100-x)(SiO_2)$ glasses [11] indicated separate Bi–O–Bi and Si–O–Si environments that form Bi_2O_3 layers and silicate chains cross-linking the layers. XAS and Raman studies of binary Bi-silicate glasses exposed to hydrogen indicate that Bi^{3+} in the initial glasses reduces to metallic Bi. XAS studies of these glasses [6–8,10] showed Bi–O correlations diminish, while Bi–Bi correlations increase with more hydrogen exposure of the melt. The original glass had Bi within environments similar to those in crystalline Bi_2O_3, while Bi-metal was observed in samples subjected to hydrogen reduction. Raman spectra of the Bi-silicate binary glasses [10] show a peak near 132 cm^{-1} assigned to Bi–O stretch motions; this feature decreases intensity with increasing hydrogen exposure time of the corresponding melt. Another narrow peak near 81 cm^{-1} (claimed to be an artifact [10]) appears in the reduced glass Raman spectra. Considering the results of the XAS studies [6–8], this 81 cm^{-1} mode may be due to Bi–Bi motions within Bi metal domains in an amorphous silica matrix. Results from these studies will be compared with XAS findings from the present study on HLW borosilicate glasses.

2. Experimental

The Bi L_{III} edge XANES and EXAFS were measured for four crystalline standards and 13 Bi-containing borosilicate samples. Phase identification of the crystalline standards was verified by powder X-ray diffraction (XRD). The crystalline standards were difficult to sieve due to static issues (especially $BiPO_4$), and the limited amounts of eulytite and bismutoferrite sample available; because of these difficulties, all standards were ground and deposited on tape without sieving, where particle sizes are $\leqslant$30 μm as measured by optical microscopy. The glass samples were synthesized as 400-g batches in Pt–Au crucibles [12,13]. The sample fragments used for XAS were taken from homogeneous portions of the annealed melt material. All glass samples were ground to powders and sieved to particle sizes less than 37 μm in diameter. According to XRD and Raman spectroscopy, the HLW-Bi-F3 through HLW-Bi-F10 glasses contain small amounts of spinel crystals or even smaller amounts of Fe-silicate phases (see Table 1) suspended in a glassy matrix. The four special Bi_2O_3-, P_2O_5-, and Cr_2O_3-variable composition glasses are completely amorphous. From XRD and SEM evidence, none of the spinel or Fe-silicate crystals contain Bi, so all Bi in these samples is in the glass matrix. Chemical analyses of the samples (Table 1) were performed by X-ray fluorescence (XRF) and direct current plasma – atomic emission spectroscopy (DCP-AES) techniques. For each XAS sample, one layer of particles was deposited on transparent tape.

The XAS data were collected at Beam Line X23-A2 at the National Synchrotron Light Source (NSLS). The synchrotron running conditions averaged near 250 mA and 2.8 GeV. Incident beam slits, down-stream of the monochromator, were set to 0.5 mm × 9 mm, resulting in an energy resolution near 2.7 eV. The spectra were gathered so that the Si (3 1 1) double-crystal monochromator was scanned from 13,020 to 13,870 eV, that included the Bi L_{III}-absorption edge near 13,419 eV. Transmission, fluorescence, and reference spectra were gathered simultaneously for each sample. The incident (I_0), transmitted (I_t), and reference (I_r) X-ray intensities were measured using three ion chambers flushed with Ar. Fluorescence X-ray intensity from the sample (I_f) was measured by a four-element Si drifted solid-state detector [14]. The axis of the solid-state detector was perpendicular with respect to the incident beam, while facing the flat sample tape placed at a 45° angle with respect to the incident beam, and between the I_0 and I_t ion chambers. Each XAS spectrum presented here is the absorption coefficient (μ) of the sample versus photon

Table 1
Major oxide compositions from XRF and DCP-AES analyses (wt.%) of the glasses. Analyses for Li and B were done by DCP-AES. Other components include: BaO, PbO, and ZrO_2. Uncertainties are within ±10% of the values reported.

Glass	Bi_2O_3	Network modifiers	Transition metals	Network formers	SO_3	Other components	Total
HLW-Bi–2Bi	11.12	CaO 0.85 Li_2O 0.15 K_2O 0.42 MgO 0.38 Na_2O 15.34	Cr_2O_3 0.71 Fe_2O_3 7.32 NiO 1.95 TiO_2 0.18 ZnO 0.17	Al_2O_3 10.31 B_2O_3 13.76 P_2O_5 5.12 SiO_2 31.42	0.30	0.46	99.96
HLW-Bi-2P	7.10	CaO 0.87 Li_2O 0.16 K_2O 0.43 MgO 0.41 Na_2O 15.22	Cr_2O_3 0.69 Fe_2O_3 7.35 NiO 1.95 TiO_2 0.17 ZnO 0.17	Al_2O_3 10.43 B_2O_3 13.84 P_2O_5 8.67 SiO_2 31.70	0.31	0.46	99.93
HLW-Bi-2P0Cr	6.92	CaO 0.91 Li_2O 0.16 K_2O 0.44 MgO 0.45 Na_2O 15.44	Cr_2O_3 0.02 Fe_2O_3 7.09 NiO 1.91 TiO_2 0.18 ZnO 0.17	Al_2O_3 10.57 B_2O_3 13.91 P_2O_5 8.72 SiO_2 32.29	0.30	0.47	99.95
HLW-Bi-P0	8.35	CaO 0.97 Li_2O 0.17 K_2O 0.49 MgO 0.38 Na_2O 16.19	Cr_2O_3 0.77 Fe_2O_3 8.46 NiO 2.28 TiO_2 0.20 ZnO 0.20	Al_2O_3 11.26 B_2O_3 15.05 P_2O_5 - SiO_2 34.26	0.36	0.55	99.94
HLW-Bi-F2[b]	8.13	CaO 0.94 Li_2O 0.16 K_2O 0.46 MgO 0.43 Na_2O 14.79	Cr_2O_3 0.77 Fe_2O_3 8.00 NiO 2.24 TiO_2 0.19 ZnO 0.21	Al_2O_3 10.91 B_2O_3 14.30 P_2O_5 5.35 SiO_2 32.11	0.40	0.52	99.91
HLW-Bi-F3[b]	7.76	CaO 0.92 Li_2O 0.16 K_2O 0.45 MgO 0.38 Na_2O 18.51	Cr_2O_3 0.73 Fe_2O_3 7.93 NiO 2.11 TiO_2 0.19 ZnO 0.17	Al_2O_3 10.66 B_2O_3 10.30 P_2O_5 5.33 SiO_2 33.44	0.37	0.49	99.90
HLW-Bi-F4[a]	7.22	CaO 0.89 Li_2O 3.16 K_2O 0.45 MgO 0.40 Na_2O 11.49	Cr_2O_3 0.67 Fe_2O_3 7.45 NiO 1.90 TiO_2 0.18 ZnO 0.17	Al_2O_3 15.46 B_2O_3 14.30 P_2O_5 5.33 SiO_2 29.99	0.36	0.46	99.88
HLW-Bi-F5R[b]	8.10	CaO 0.98 Li_2O 0.18 K_2O 0.47 MgO 0.40 Na_2O 17.81	Cr_2O_3 0.77 Fe_2O_3 8.32 NiO 2.19 TiO_2 0.20 ZnO 0.19	Al_2O_3 12.79 B_2O_3 11.33 P_2O_5 5.87 SiO_2 29.41	0.39	0.52	99.92
HLW-Bi-F6[a,b]	7.17	CaO 3.95 Li_2O 3.16 K_2O 0.43 MgO 0.36 Na_2O 11.55	Cr_2O_3 0.68 Fe_2O_3 7.47 NiO 1.95 TiO_2 0.17 ZnO 0.17	Al_2O_3 14.54 B_2O_3 14.30 P_2O_5 5.36 SiO_2 27.86	0.35	0.47	99.93
HLW-Bi-F7[a,b]	8.68	CaO 1.06 Li_2O 0.19 K_2O 0.53 MgO 0.39 Na_2O 17.15	Cr_2O_3 0.82 Fe_2O_3 8.90 NiO 2.30 TiO_2 0.21 ZnO 0.20	Al_2O_3 12.89 B_2O_3 11.36 P_2O_5 6.47 SiO_2 27.74	0.45	0.56	99.90
HLW-Bi-F8[b]	8.22	CaO 1.00 Li_2O 0.18 K_2O 0.49 MgO 0.40 Na_2O 18.58	Cr_2O_3 0.76 Fe_2O_3 8.41 NiO 2.24 TiO_2 0.20 ZnO 0.19	Al_2O_3 11.80 B_2O_3 10.33 P_2O_5 5.82 SiO_2 30.40	0.36	0.55	99.93
HLW-Bi-F9[a]	6.90	CaO 0.92 Li_2O 5.16 K_2O 0.45 MgO 0.35 Na_2O 8.64	Cr_2O_3 0.62 Fe_2O_3 7.01 NiO 1.78 TiO_2 0.18 ZnO 0.16	Al_2O_3 14.78 B_2O_3 16.30 P_2O_5 5.54 SiO_2 30.28	0.38	0.43	99.88
HLW-Bi-F10[a]	7.61	CaO 0.99 Li_2O 5.18 K_2O 0.51 MgO 0.40 Na_2O 8.90	Cr_2O_3 0.57 Fe_2O_3 7.77 NiO 1.94 TiO_2 0.17 ZnO 0.18	Al_2O_3 13.95 B_2O_3 15.33 P_2O_5 6.07 SiO_2 29.34	0.52	0.50	99.91

[a] Indicates samples with spinel crystals.
[b] Indicates samples with possible crystalline Fe-silicate phases.

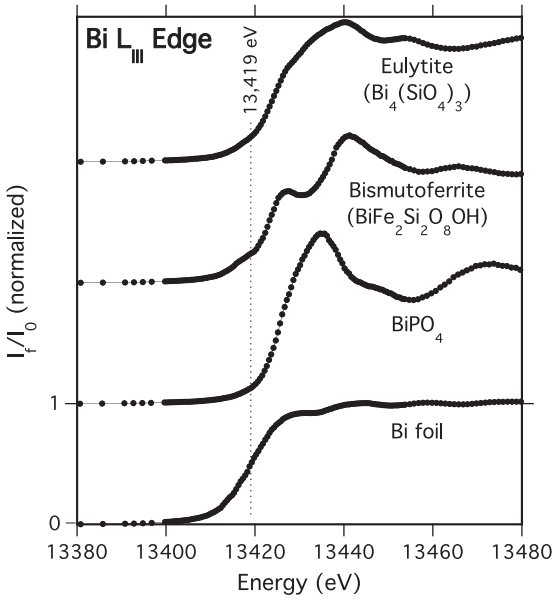

Fig. 1a. Edge-step normalized Bi L_{III} XANES spectra of the standards, where E_0 is set to 13,419 eV. Plots are offset for clarity.

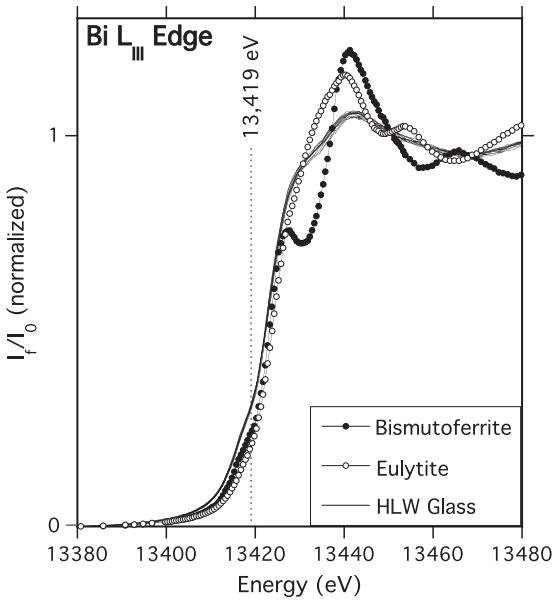

Fig. 1b. Edge-step normalized Bi L_{III} XANES spectra of the thirteen glasses studied (lines) and the two Bi-silicate standards: eulytite and bismutoferrite (points and lines).

energy, where μ is proportional to I_f/I_0. To calibrate the Bi L_{III}-edge energy in each X-ray fluorescence spectrum, the transmission spectrum of a Bi foil was taken simultaneously; the foil was placed between the I_t and I_r ion chambers down-stream of the sample.

3. Data analysis

The fluorescence XANES spectra presented are averages of at least four data sets from each sample that were initially processed using standard pre-edge background subtraction and edge-step normalization procedures [5]. The energy at the derivative maximum of the Bi L_{III}-absorption edge for Bi foil was calibrated to 13,419 eV, and defined as E_0 (Figs. 1a and 1b) [16]. Self-absorption corrections to the fluorescence XANES and EXAFS standards data were done using the programs FLUO [17] and SABCOR [18],

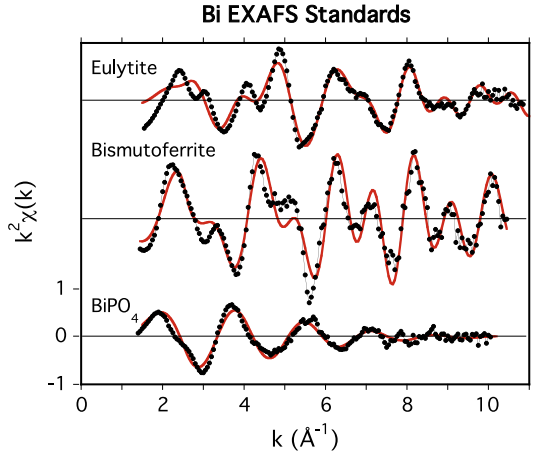

Fig. 2a. Bi L_{III} EXAFS for the standards: data (points and line) and fit (red line). Plots are offset for clarity. (For interpretation of the references to color in this figure legend, the reader is referred to the web version of this article.)

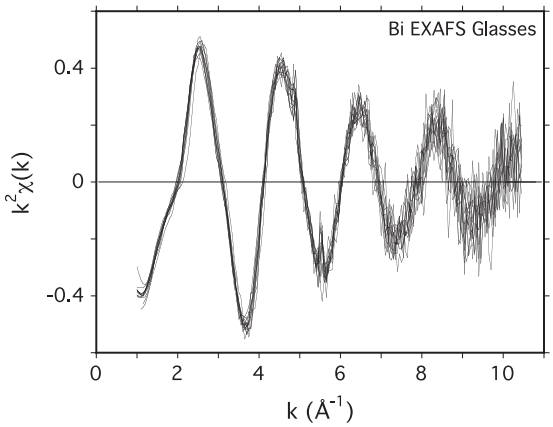

Fig. 2b. Bi L_{III} EXAFS data for the 13 borosilicate glasses investigated. The small, narrow features at 4.9 and 5.5 Å^{-1} are monochromator artifacts.

respectively. Self-absorption effects to the spectra are larger for the more Bi-concentrated eulytite and $BiPO_4$ samples, and minimal for bismutoferrite. After normalization and calibration, direct comparisons can be made with XANES data for all samples to an energy accuracy of +0.5 eV, or the energy difference between two adjacent data points at the edge (Figs. 1a and 1b). A cubic spline function was fit to and then subtracted from the edge-step normalized data. Energy values in eV were converted to k (Å^{-1}) [15], where the resulting $\chi(k)$ data was k^2-weighted (Figs. 2a, 2b, and 4 (bottom)). The $k^2\,\chi(k)$ data were then Fourier-transformed over the $2.0 < k < 10.4$ Å^{-1} range, where a 1.0 Å^{-1} Hanning window was used on the upper and lower limits of the data to minimize Fourier-transform termination artifacts in the resulting partial radial distribution function (RDF). Peaks in the RDFs correspond to shells of atoms surrounding Bi (Figs. 3a, 3b, and 4 (top)), where r, n, and σ^2 for each atomic shell can be obtained from the fitting procedure [19]. The position of each peak in the RDF is phase-shifted to lower r by approximately 0.3–0.5 Å with respect to the actual average bond distance that corresponds to each peak. The RDF fitting range to include the nearest-neighbor peaks was from 1.0 to 4.2 Å for eulytite, 1.0 to 3.7 Å for bismutoferrite, 0.9 to 2.2 Å for $BiPO_4$, and 1.0 to 2.1 Å for the glasses.

Atom clusters, surrounding a central Bi atom to a maximum radial distance of 5 Å, were generated to simulate the eulytite, bismutoferrite, and $BiPO_4$ structures [2,3,5]. These clusters were used by IFEFFIT [19] to calculate the theoretical EXAFS for each

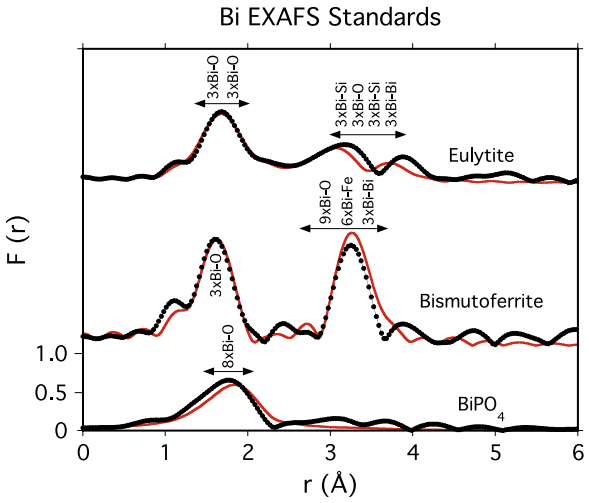

Fig. 3a. Partial RDFs for the standards: data (points and line) and fit (red line). Important pair correlations calculated by FEFF7.02 from the crystal structures are indicated near the appropriate features. Plots are offset for clarity. (For interpretation of the references to color in this figure legend, the reader is referred to the web version of this article.)

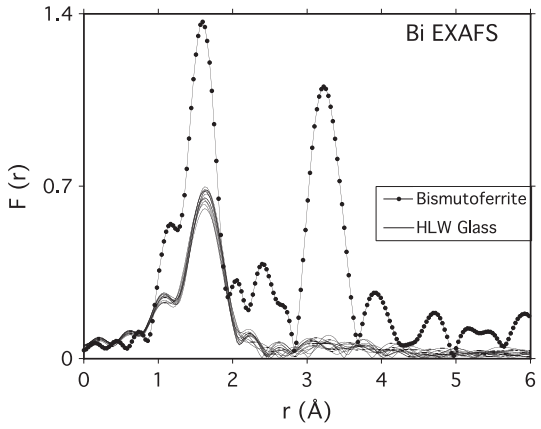

Fig. 3b. Partial RDFs for the 13 borosilicate glasses and the Bi-silicate standard bismutoferrite.

standard. By taking into account the important atom correlations calculated by FEFF from the atom clusters, Bi–O, Bi–Si, and Bi–Bi path contributions could then be used to label the peaks in the partial RDFs for the standards (Fig. 3a).

Eulytite was the first analyzed standard, because it is the simplest chemistry Bi-silicate that would be a realistic structural approximation to the Bi environments in the glasses. Five paths were used to describe most of the features in the $k^2\chi(k)$ data and resulting RDF (Figs. 2a (top) and 3a (top), Table 2). The dominant contributions to the theoretical X-ray absorption spectrum for eulytite are the two Bi–O nearest-neighbor single scattering paths at 2.15 and 2.62 Å [2], and other paths contributing to the two RDF peaks near 3.1 and 3.9 Å (Fig. 3a (top)), that include Bi–Si at 3.54 and 3.59 Å, as well as Bi–Bi at 3.83 Å. The fitting routine behaved more stably by fitting all RDF peaks below 4.2 Å. Initially, all Bi distances and coordination numbers ($n = 3$ for all paths) were constrained to their actual values, while E_0, s_0^2 (a scaling factor that includes EXAFS amplitude damping effects [15]), and σ^2 for the Bi–O paths were varied. In the final fitting procedure, r, n, and σ^2 were varied for the nearest neighbor Bi–O paths as well as r-values for the Bi–Si and Bi–Bi contributions, while E_0 and s_0^2 were constrained to 13,420.4 eV (or 1.4 eV from E_0) and 1.00, respectively. Due to the multiple contributions and highly correlated n

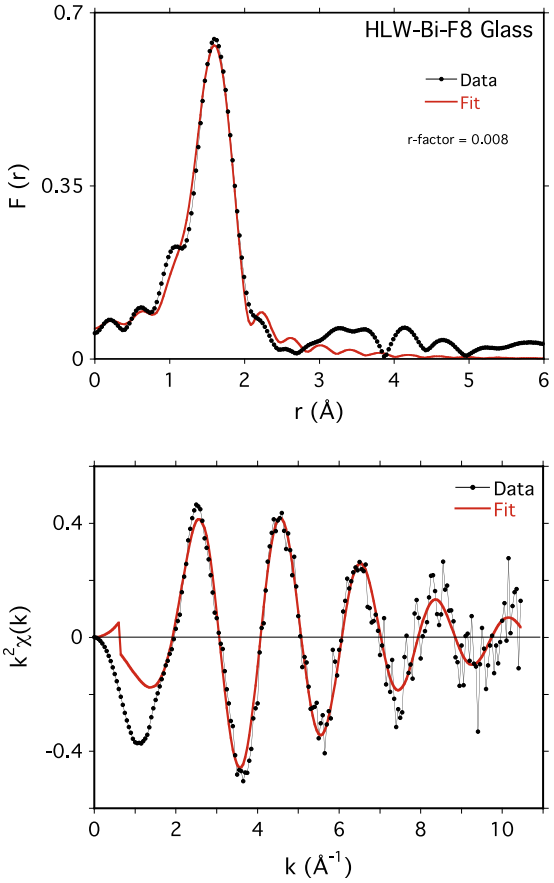

Fig. 4. RDF and $k^2\chi(k)$ data (points and line) and fit (red line) for a representative glass. (For interpretation of the references to color in this figure legend, the reader is referred to the web version of this article.)

Table 2
Bi-O nearest-neighbor fitting results for the standards. The r-factor is a goodness of fit parameter that is a sum-of-squares measure of the fractional misfit scaled to the magnitude of the data [19]. Average values are listed with averaged uncertainties (in parentheses) calculated by IFEFFIT. All fits used: $s_0^2 = 1.00$ and $E_0 = 1.4$ eV.

Standard	r-factor	r (Å)	n (atoms)	σ^2 (Å^2)
Eulytite ($Bi_4Si_3O_{12}$)				
Bi–O fit	0.100	2.15 (0.02)	3.5 (2.1)	0.0037 (0.0061)
Bi–O actual [2]		2.15	3.0	
Bi–O fit		2.61 (0.03)	3.0 (3.8)	0.0059 (0.0160)
Bi–O actual		2.62	3.0	
Bi–Si fit		3.52 (0.03)	3.0[a]	0.0024[a]
Bi–Si actual		3.54	3.0	
Bi–Si fit		3.66 (0.04)	3.0[a]	0.0024[a]
Bi–Si actual		3.59	3.0	
Bi–Bi fit		3.83 (0.03)	3.0[a]	0.0024[a]
Bi–Bi actual		3.82	3.0	
Bismutoferrite ($BiFe_2Si_2O_8OH$)				
Bi–O fit	0.103	2.14 (0.02)	4.2 (1.2)	0.0018 (0.0029)
Bi–O actual [3]		2.11	3.0	
Bi–O fit		3.37[a]	7.0[a]	0.0080[a]
Bi–O actual		3.37	7.0	
Bi–O fit		3.62[a]	2.0[a]	0.0020[a]
Bi–O actual		3.62	2.0	
Bi–Fe fit		3.70[a]	6.0[a]	0.0016[a]
Bi–Fe actual		3.70	6.0	
Bi–Si fit		4.00[a]	6.0[a]	0.0016[a]
Bi–Si actual		4.00	6.0	
$BiPO_4$				
Fit	0.008	2.44 (0.01)	7.6 (0.9)	0.0189 (0.0026)
Actual [5]		2.50	8.0	

[a] Indicates a constrained parameter.

and σ^2 parameters, only r was varied for the two Bi–Si and single Bi–Bi paths in the final fitting (Table 2). In all fitting routines, E_0 and s_0^2 were constrained to the above values.

The bismutoferrite fitting included RDF features from 1.0 to 3.7 Å and used five paths to describe the main features in the $k^2\chi(k)$ data and corresponding RDF peaks near 1.60 and 3.25 Å (Figs. 2a (middle), 3a (middle), and Table 2). The first-shell RDF peak could be stably fit by varying r, n, and σ^2 for the 2.05 Å Bi–O path in the bismutoferrite crystal structure model. The 3.7 Å RDF peak can be best described using the 3.66 Å Bi–Fe and 4.00 Å Bi–Si paths; however, two Bi–O correlations were also used to provide a better fit to this RDF peak. The 3.37 Å Bi–O path using a large Debye-Waller factor was included to describe the continuum of seven Bi–O distances from 3.27 to 3.53 Å, while another 3.61 Å Bi–O path was used to account for two Bi–O correlations at that same distance. Since twelve parameters describe the four paths used to fit the 3.7 Å RDF peak, the highly correlated r, n and s^2 variables for each path were all constrained to values that are reasonable descriptions of the crystal structure around Bi, so that IFEFFIT could stably fit most of the features in the EXAFS data.

The first-shell RDF peak for $BiPO_4$ was fit by varying r, n, and σ^2 for the 2.05 Å Bi–O path in the bismutoferrite crystal structure model (Table 2, and Figs. 2a (bottom) and 3a (bottom)); the same routine was used to fit the first-shell peak near 1.7 Å in the RDFs for the glasses (Table 3, and Figs. 3b and 4 (top)). "Multi-electron resonance effects" were reported at approximately 200 eV above the Bi L_{III} edge in the EXAFS for liquid Bi and Bi_2O_3 [20]. However, no such features were found near 8.7 $Å^{-1}$ ($E - E_0 \sim 200$ eV) in the $k^2\chi(k)$ data (Figs. 2a and 2b), where EXAFS fitting describes the major features in the $k^2\chi(k)$ and RDF data (Figs. 2a, 3a, and 4).

4. Discussion

4.1. Bi L_{III} XANES data

The XANES spectra for the standards show an edge shift to higher energies (typically measured half way up the edge step, at $\mu = 0.5$) by approximately 4–5 eV from Bi-foil to the Bi^{3+} standards, eulytite, bismutoferrite, and $BiPO_4$ (Fig. 1a). XANES for the Bi^{3+} standards are significantly different from one another reflecting the different crystal structures surrounding Bi in these cases. The $BiPO_4$ spectrum has a relatively sharp (10 eV width) edge-peak near 13,435 eV, that is not present in the XANES for the two Bi-silicates.

All glass spectra are nearly identical and most similar to the XANES for eulytite (Fig. 1b). The glass data show Bi^{3+} as the dominant Bi species, where there is no evidence for Bi-metal or Bi-phosphate domains. The glass spectra have relatively broad features compared with their crystalline Bi-silicate counterparts, which indicate more static disorder of the arrangement of atoms around Bi in the glass structures than in the crystalline standards.

Table 3
First-shell Bi–O fitting results for all glasses investigated. Conventions in Table 2 are used.

Glass	r-factor	r (Å)	n (atoms)	σ^2 (Å^2)
HLW-Bi-2P	0.018	2.14 (0.01)	2.5 (0.4)	0.0075 (0.0026)
HLW-Bi-P0	0.029	2.13 (0.01)	2.6 (0.6)	0.0067 (0.0035)
HLW-Bi-2P0Cr	0.018	2.13 (0.01)	2.5 (0.4)	0.0072 (0.0025)
HLW-Bi-2Bi	0.010	2.13 (0.01)	2.7 (0.3)	0.0068 (0.0019)
HLW-Bi-F2	0.030	2.13 (0.01)	2.4 (0.5)	0.0049 (0.0033)
HLW-Bi-F3	0.022	2.13 (0.01)	2.7 (0.5)	0.0073 (0.0032)
HLW-Bi-F4	0.036	2.12 (0.01)	2.7 (0.7)	0.0073 (0.0041)
HLW-Bi-F5r	0.024	2.13 (0.01)	2.6 (0.5)	0.0072 (0.0033)
HLW-Bi-F6	0.026	2.13 (0.01)	2.9 (0.6)	0.0086 (0.0037)
HLW-Bi-F7	0.053	2.12 (0.01)	2.5 (0.7)	0.0063 (0.0045)
HLW-Bi-F8	0.008	2.13 (0.01)	2.7 (0.3)	0.0078 (0.0019)
HLW-Bi-F9	0.036	2.13 (0.01)	2.6 (0.7)	0.0062 (0.0038)
HLW-Bi-F10	0.042	2.13 (0.01)	2.4 (0.6)	0.0052 (0.0035)

4.2. EXAFS data and analysis

4.2.1. Standards

The $k^2\chi(k)$ data for the standards (Fig. 2a) show significant differences between the Bi-silicates and $BiPO_4$, reflecting the different atomic arrangements surrounding Bi in these phases. The data for $BiPO_4$ has one damped single frequency component that Fourier transforms to the broad nearest-neighbor peak in the RDF (Fig. 3a (bottom)), due to the continuum of eight Bi–O nearest-neighbor distances. Data for both Bi-silicates contain relatively complicated oscillations that indicate contributions from first- and second-nearest neighbors, as well as more distant correlations, shown in the corresponding RDFs (Fig. 3a (top two plots)). These silicate structures have narrower ranges of distances from Bi compared with the $BiPO_4$ structure.

Fitting results for the standards (Figs. 2a and 3a) describe most features in the $k^2\chi(k)$ data and corresponding partial RDFs. The results for eulytite indicate that the relatively damped nearest-neighbor peak is due to the two sets of Bi–O nearest-neighbor distances, where final r and n values are reasonably close to the actual values from the crystal structure refinement (Table 2) [2]; the relatively weak RDF peaks between 4 and 5 Å can be explained by a series of Bi–O, Bi–Si, and Bi–Bi correlations. The results for bismutoferrite indicate that the first shell peak near 1.7 Å is due to the nearest three oxygen atoms from the $FeO_4(OH)_2$ octahedral layer (Table 2) [3]. The 3.2 Å RDF peak can be mostly fit by Bi–Fe and Bi–Si contributions, as well as the continuum of nine Bi–O correlations from 3.28 to 3.62 (Table 2). The first-shell fitting results for $BiPO_4$ include a large Debye–Waller factor, consistent with the continuum of eight coordinating oxygens in the Bi-site. The shorter 2.44 Å Bi–O distance determined from EXAFS with respect to the average Bi–O of 2.50 Å from the crystal structure determination [5] indicates that EXAFS probably detects the shorter Bi–O contributions and can miss the more distant oxygens in a positionally disordered Bi-site, as seen earlier for Na-sites in silicates (20,21).

4.2.2. Crucible and melter glasses

The $k^2\chi(k)$ data for the glasses investigated are all similar (Fig. 2b), and are dominated by one damped frequency component. The corresponding RDFs are dominated by one nearest-neighbor peak near 1.6 Å that more closely corresponds with the nearest-neighbor RDF peaks for eulytite and bismutoferrite (Figs. 3a and 3b) than the peak near 1.8 Å for $BiPO_4$ (Fig. 3a). The small, broad features between 3 and 4.5 Å (Figs. 3b and 4 top) are probably due to second nearest-neighbor correlations (Bi–Si, for example) and are too weak to reliably determine structural parameters from the fitting. Therefore, Bi EXAFS for all glasses investigated exhibit no significant changes with respect to glass chemistry, including the samples with specific variations in Cr, P, or Bi content.

Fitting one Bi–O nearest-neighbor correlation to the glass EXAFS data describes virtually all features in the $k^2\chi(k)$ data and partial RDFs (Fig. 4). The RDF features and fitting results indicate Bi–O distances within 0.02 Å of 2.13 Å for the glasses (Fig. 4 and Table 3) or close to the Bi–O nearest-neighbor distances determined for eulytite and bismutoferrite. These results indicate that the glasses have significantly shorter Bi–O distances than the average 2.44 Å Bi–O nearest-neighbor distance in $BiPO_4$. The glass EXAFS analyses (Table 3 and Fig. 4) indicate that the average Bi environment in the glasses can be considered a disordered version of the Bi-site in eulytite or bismutoferrite, where the EXAFS signal is dominated by the nearest three oxygens. The more distant oxygens within these Bi-sites are probably positionally disordered enough to contribute little or nothing to the EXAFS [21]; similar limitations

in EXAFS analysis results were observed for Na-sites in silicates [22].

Comparisons of the above EXAFS findings with the earlier Bi XAS work [6–8] indicate some similarities between the Bi–O nearest-neighbor environments in the HLW glasses and binary Bi-silicate glasses. The EXAFS data, as well as the determined Bi–O distances (r = 2.12–2.14 Å) and coordination numbers (n = 3.0) for the unreduced binary glasses [6] are similar to the $k^2\chi(k)$ data and analysis results shown in Fig. 2b and Table 3, respectively. Bi EXAFS data also show no evidence of Bi–Bi correlations in the HLW glasses that were evident in the X-ray scattering RDFs determined for $50(Bi_2O_3) \cdot 50(SiO_2)$ glass [11]. This lack of Bi-clustering in the HLW glasses would be expected in light of their compositions, because of the much lower Bi^{3+} concentrations in the HLW glass structures than in the binary Bi-silicate glass structure [11].

5. Conclusions

Bismuth XAS data were collected for Bi-foil, three crystalline standards, and thirteen borosilicate waste glasses. Bi XANES data for all glasses are nearly identical and similar to the XANES of the Bi-silicate standard, eulytite indicating Bi^{3+} is likely surrounded by oxygen atoms from silicate tetrahedra. First-shell EXAFS analyses for all glasses resulted in average Bi–O distances near 2.13Å, coordination numbers near three, and indicate that Bi is probably within a disordered version of the Bi-site in eulytite and bismutoferrite. In these glass structures, the EXAFS data most likely sense only the nearest three oxygens around Bi. The EXAFS determined Bi–O nearest-neighbor distances indicate that Bi in the glasses is most likely surrounded by oxygens from the silicate network and *not* phosphate tetrahedra. No XAS evidence was observed for metallic Bi or Bi–O–Bi bonding in any of the glass samples investigated. XANES and EXAFS also indicate that the Bi nearest-neighbor environments in HLW borosilicate samples are remarkably similar despite the different glass compositions and different melt foaming behaviors. The possible link between Cr behavior in these borosilicates and melt foaming will be more specifically addressed in a follow-up Raman spectroscopy and Cr XAS study [9].

Acknowledgments

We thank J.E. Post and P. Pohwat (Mineral Sciences Department, National Museum of Natural History, Smithsonian Institution) for supplying the bismutoferrite and eulytite samples. We also thank Cecilia Zischkau (Summer Intern, Vitreous State Laboratory) for preparing the HLW glass samples used in the XAS experiments and for collecting the XRD data for the same samples. We appreciate the help from J.C. Woicik (NIST) and George Sterbinsky (NSLS, NIST) for arranging the beam time and assistance with the experimental set-up at NSLS Beam Line X23-A2. This work was supported in part by the US Department of Energy Office of River Protection through Energy *Solutions*, Inc.

References

[1] K.S. Matlack, H. Gan, W.K. Kot, M. Chaudhuri, R.K. Mohr, D.A. McKeown, T. Bardakci, W. Gong, A.C. Buechele, I.L. Pegg, I. Joseph, Tests with High-Bismuth HLW Glasses, Final Report, VSL-10R1780-1, Rev 0, Vitreous State Laboratory, The Catholic University of America, Washington, DC, December 2010.
[2] D.J. Segal, P.P. Santoro, R.E. Newnham, Z. Kristallogr. 123 (1966) 73.
[3] A.P. Zukhlistov, B.B. Zvjagin, Kristallogr. 22 (1977) 731.
[4] J. Ketterer, V. Kramer, Neues Jahrbuch für Mineralogie Monatschefte H1 (1986) 13.
[5] B. Romero, S. Bruque, M.A.G. Aranda, J.E. Iglesias, Inorg. Chem. 33 (1994) 1869.
[6] A. Witkowska, J. Rybicki, A. DiCicco, J. Alloys Compd. 401 (2005) 135.
[7] A. Witkowska, J. Rybicki, L. Murawski, A. DiCicco, Mol. Phys. Reports 36 (2002) 133.
[8] A. Witkowska, J. Rybicki, A. DiCicco, Phys. Chem. Glasses 43C (2002) 124.
[9] D.A. McKeown, H. Gan, I.L. Pegg, J. Nucl. Mater. in preparation.
[10] Z. Pan, D.O. Henderson, S.H. Morgan, J. Non-Crystalline Solids 191 (1984) 134.
[11] T. Namba, H. Tabachi, Y. Muira, Structure of Bi_2O_3–SiO_2 glasses, Ph.D. Thesis, Department of Environmental Chemistry and Materials, Okayama University, 2004.
[12] K.S. Matlack, H. Hojaji, S.S. Fu, I.L. Pegg, P.B. Macedo, Cer. Trans. 61 (1995) 221.
[13] S.S. Fu, W. Luo, H. Hojaji, M. Brandys, R.K. Mohr, K.S. Matlack, I.L. Pegg, P.B. Macedo, Cer. Trans. 72 (1996) 27.
[14] J.C. Woicik, B. Ravel, D.A. Fischer, W.J. Newburgh, J. Synchrotron Rad. 17 (2010) 409.
[15] D.E. Sayers, B.A. Bunker, in: D.C. Kroningsberger, R. Prins (Eds.), X-ray absorption principles, applications, techniques of EXAFS, SEXAFS, and XANES, Wiley, New York, 1988. pp. 211 (Chapter 6).
[16] B. Ravel, M. Newville, J. Synchrotron Rad. 12 (2005) 537.
[17] D. Haskel, 1999. The executable code and documentation can be accessed at: <www.aps.anl.gov/xfd/people/haskel/fluo.html>.
[18] C.H. Booth, F. Bridges, Phys Scripta T115 (2005) 202.
[19] M. Newville, J. Synchrotron Rad. 8 (2001) 322.
[20] A. DiCicco, A. Filipponi, Phys. Rev. B49 (2002) 12564.
[21] P. Eisenberger, G.S. Brown, Solid State Commun. 29 (1979) 481.
[22] D.A. McKeown, G.A. Waychunas, G.E. Brown Jr, J. Non-Crystalline Solids 74 (1985) 325.